

Motion Behavior of Nonmetallic Inclusions at the Interface of Steel and Slag. Part I: Model Development, Validation, and Preliminary Analysis



CHAO LIU, SHUFENG YANG, JINGSHE LI, LIBIN ZHU, and XIAOGANG LI

The motion behavior of nonmetallic inclusions at the interface of molten steel and slag fundamentally affects the removal of inclusions. Therefore, from an analysis of forces, this study constructed a mathematical model of inclusion movement. Compared with other models that only consider the forces acting on nonmetallic inclusions at the interface, the proposed model considers not only cases in the inclusions which enter the slag interior and rebound into the molten steel, but also the effect of fluid flow containing the inclusions with different Re numbers on the drag force. The application of this established model has not taken Reynolds number of fluid flow into consideration. The model can predict the motion of inclusions at the interface and in nearby areas and provide a curve of inclusion displacement vs time. The mathematical model was verified with a physical model, with the curve of displacement vs time obtained from physical experiment being consistent with the calculated curve. The preliminary calculation results show that inclusions having liquid film at their surfaces are rebounded into the steel when they have size within a certain range but enter the slag phase directly when they are beyond that size range.

DOI: 10.1007/s11663-016-0605-1

© The Author(s) 2016. This article is published with open access at Springerlink.com

I. INTRODUCTION

THE progress of science and technology has produced steel of higher quality. Nonmetallic inclusions are generally considered to adversely affect the performance of steel.^[1] Nonmetallic inclusions are usually classified into two categories:^[2] residual products resulting from alloying elements intentionally added for de-oxidation in the ladle and products resulting from reactions between the melt and the atmosphere or slag.

Inclusions in metallic melts are often removed through capture by the slag phase, which is usually a molten mixture of metal oxides. In the manufacturing process, this may occur in the ladle, tundish, or mold. Lee and Sridhar^[3] described the separation of inclusion in three steps: (i) the floating of inclusions to the steel–slag interface, (ii) separation into the slag phase through the interface, and (iii) dissolution into the slag phase. There have, over the years, been several attempts to study the floating process and dissolution process. Wikstrom and Nakajima^[4] investigated the effect of the

particle size (5 to 200 μm) of inclusions in soft blow flow on separation efficiency. Ramos-Banderas^[5] studied the trajectories of inclusions of different particle size with a Eulerian–Lagrangian stochastic trajectory model. Wang^[6] studied the inclusion trajectory and separation rate when blowing argon or employing electromagnetic braking. Hallberg^[7] and Miki *et al.*^[8] presented models of inclusion growth and separation. Many works^[9–12] have described the thermodynamics of inclusion removal. However, most of these models and studies argue that inclusions are separated and eliminated once they reach the interface between steel and slag.

The second step of separating inclusions into slag has been hardly noticed. Nakajima and Okamura^[13–15] put forward models predicting the separating process for nonmetallic inclusions. In the models, the particle at the interface between steel and slag is subject to four forces: the buoyancy force, added force, rebound force, and drag force. The models indicate that the overall wettability should be positive and that the slag viscosity should be as low as possible to obtain the most favorable conditions for inclusion transfer at the steel–slag interface. Cleaver and Yates^[16] put forward a turbulent bursting model combined with the inclusion model by Nakajima and Okamura.^[13] Valdez and Shannon^[17] calculated the capture of inclusions at the interface between molten iron and different slags using the model proposed by Nakajima.^[15] Bouris and Bergeles^[18] considered that inclusions can pass into the slag layer and avoid re-entrainment, as the interfacial tension between slag and inclusion should be less than that between steel and inclusion, but inclusion particles that reach an equilibrium state at the steel–slag interface are subject to re-entrainment back into the steel, owing

CHAO LIU, Ph.D. Student, formerly with the State Key Laboratory of Advanced Metallurgy, University of Science and Technology Beijing, Beijing, and is now with the Corrosion and Protection Center, University of Science and Technology Beijing, Beijing 100083, P.R. China. SHUFENG YANG, Associate Professor, JINGSHE LI, Professor, and LIBIN ZHU, Ph.D. Student, are with the School of Metallurgical and Ecological Engineering, University of Science and Technology Beijing, Beijing 100083, China. XIAOGANG LI, Professor, is with the Corrosion and Protection Center, University of Science and Technology Beijing, Beijing 100083. Contact eTechnology Beijing, Beijing-mail: yangshufeng@ustb.edu.cn

Manuscript submitted February 22, 2015

Article published online February 16, 2016.

to the turbulent boundary layer at the interface. They therefore introduced shear stress into the model.

The models above clearly describe the forces acting on inclusions but are exclusive of forces acting on inclusions in steel phase, in slag phase or near the interface. When the inclusion oscillates at the interface, it may enter the steel phase or slag phase completely and its forces will thus be different. Inclusions of certain sizes may rebound into steel before film rupture, and then move to the interface and separate into the slag phase; in this case, the model is inaccessible. This study presents a novel analysis of the (delete) changing forces when inclusions are in steel phase, slag phase, at the interface between steel and slag, and in a continuous process during separation. Consequently, this further analysis may affect the motion trail and separation time.

Moreover, the aforementioned models, especially the one in References 14 and 15, assume the flowing fluid containing the inclusions is Stokes flow regardless of the value of Re (Reynolds number). The research of Davila,^[18] Morales,^[19] and Cukierski^[20] indicates that there are 3 different Re values (0.98, 2.86, 15.91) of a 50 μm inclusion in Ladle, Tundish, and Mold at different fluid flow speed. Researchers^[21] indicated that when $Re > 8$, standing eddies appear behind the inclusions, furthermore it causes uneven pressure around the inclusions. If the Re is big enough, inclusions oscillate in the process of movement, the drag force acting on the inclusion transforms into Newton viscous resistance force.

The first part of this study establishes a mathematical model of the motion behavior of nonmetallic inclusions at the interface of molten steel and slag and verifies the mathematical model with a physical model. Preliminary calculation results are then analyzed.

The second part presents results on the effects of inclusion size, interfacial tension between the inclusion and slag phase, and viscosity of slag on the motion behavior of inclusions at the steel–slag interface according to the mathematical model.

II. THEORETICAL MODEL

This research optimizes the mathematical model of inclusions movement at the interface between slag and metal according to the model of Nakajima and Strandh.^[13–15] The movement of inclusions at the steel–slag interface is shown in Figure 1. The figure has ordinate Z and abscissa t . The abscissa is drawn along the direction of the steel–slag interface, and shows the movement of inclusions at the steel–slag interface with time. The ordinate Z is perpendicular to the interface of steel and slag, and thus shows the displacement of inclusions at the steel–slag interface. Z is a function of time t , and thus denoted as $Z(t)$. When inclusions arrive at the steel–slag interface (as shown by position 2 in Figure 1), initial time $t_0 = 0$ and initial displacement $Z_0 = 0$. There are four possibilities for the movement of an inclusion at the steel–slag interface. 1) After arriving at the steel–slag interface, the inclusion directly passes through the interface into the slag layer; the process is described in Figure 1 by 1→2→4→5. 2) After arriving at

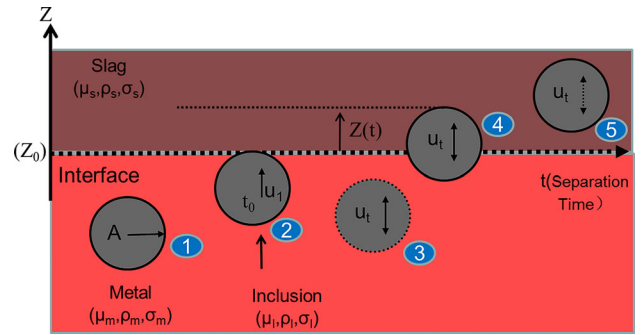


Fig. 1—Schematic of inclusion motion at the steel–slag interface.

the steel–slag interface, the inclusion does not fully penetrate the interface but oscillates the steel–slag interface, and finally remains at the steel–slag interface; the process is described by 1→2→4. 3) After arriving at the steel–slag interface, the inclusion does not fully penetrate the interface but rebounds into the liquid steel, and then floats upward to reach the steel–slag interface under the action of buoyancy, finally completing separation; the process is described by 1→2→3→4→5. 4) After arriving at the steel–slag interface, the inclusion does not fully penetrate the interface but rebounds into the liquid steel and then floats upward and arrives at the steel–slag interface, oscillating the steel–slag interface, and finally remaining at the steel–slag interface; the process is described by 1→2→3→4. All four cases of inclusion movement at the steel–slag interface include three or more consecutive stages, with the three basic stages being the inclusion in liquid steel, the inclusion in the two-phase steel–slag zone, and the inclusion in the slag phase.

The forces acting on the inclusion are not the same in the different stages of movement. Force analysis should be carried out for each stage of continuous inclusion movement. According to the inclusion location, the force distribution of inclusions is determined at that moment. Then, according to the force situation of inclusion movement at the steel–slag interface at different stages, the relationship between inclusion displacement and time can be constructed according to Newton's law, and a mathematical model of inclusion movement at the steel–slag interface can be established. The mathematical model established in this research considers all stages of the inclusion movement at and near the steel–slag interface. The behavior of inclusion movement in and near the steel–slag interface, the possibility of a rebound phenomenon occurring in the process of inclusion movement through the interface and corresponding influencing factors are studied in detail. According to the Nakajima's^[13–15] model, the following assumptions are made in building this optimized model. The inclusion volume is fixed and solid, and the slag phase is liquid. The inclusions do not react with the slag. All fluid is incompressible and isothermal. All interface parameters are constant. Buoyancy, resistance, and rebound force as well as surface tension affect inclusions at and near steel–slag interface, when $Z(t)$ is greater than twice of the inclusion radius after the film breakup, the inclusions are considered as completely out

of steel–slag and enter into the slag phase. According to the research of Nakajima and Okamura,^[13] there are two cases where inclusions float upward and arrive at the steel–slag interface depending on whether the inclusions are attached to the steel liquid film. The Re of inclusion movement determines whether there is a steel liquid film. There is a liquid film when $Re > 1$ but not when $Re < 1$. When inclusions arrive at the steel–slag interface, a liquid film is produced or the slag, steel, and inclusion triple phases contact directly without a liquid film. In both cases, inclusions pass through the steel–slag interface or stay at the steel–slag interface under the effects of the rebound, buoyancy, resistance, and added-mass forces. However, the forces will differ if there is no liquid film. Force analysis is required for both conditions of whether there is a liquid film or not.

In this research, force is analyzed by dividing into three parts during the inclusions moving process—near the interface, completely in the metal phase, and slag phase. Although both in the metal phase and slag phase are important to a continuous inclusions separating process, they are not considered in the previous research. In the whole process of movement, the drag force changes with the change of Re number. When $Re < 8$, the flowing fluid containing the inclusions at the steel–slag interface is all regarded as Stokes flow. When Re is larger than 500, the flow condition meets Newton’s law, thus the drag force acting on the inclusion transforms into Newton viscous resistance force. As Re range from 8 to 500, actually no determinate formula can be applied to calculate the drag force. So this research selects Schiller–Nauman’s empirical formula with a minimum error ranging between calculating and experimental result -4 to $+5$ pct.^[22]

When Re is less than 8, the drag force acting on the inclusion is defined as:

$$F_d = 6\pi A \mu_S \cdot \tilde{B} \cdot \frac{dZ}{dt}, \quad [1]$$

When Re is between 8 and 500, the drag force acting on the inclusion is defined as:

$$F_d = 6\pi \mu_S \cdot \tilde{B} \cdot A (1 + 0.15 Re^{0.687}) \frac{dZ}{dt}, \quad [2]$$

When the Re is larger than 500, the drag force affected on the inclusion is defined as:

$$F_d = 0.22\pi \rho_S \cdot \tilde{\Delta}_b \cdot \left(\frac{dZ}{dt}\right)^2 A^2, \quad [3]$$

where:

$$\tilde{B} = \begin{cases} \frac{\mu_M}{\mu_S} \\ \left(\frac{\mu_M}{\mu_S} - 1\right) \left(\frac{Z}{R}\right)^2 - 2\left(\frac{\mu_M}{\mu_S} - 1\right) \left(\frac{Z}{R}\right) + \frac{\mu_M}{\mu_S} & 0 \leq \frac{Z}{A} \leq 1 \\ 1 & \frac{Z}{A} > 1 \end{cases} \quad [4]$$

$\tilde{\Delta}_b$ is a fractionalized density term that weighs the particular absolutely and after it transfers into the effects of each outside phase:

$$\tilde{\Delta}_b = \begin{cases} 1 & Z > 2A \\ \frac{1}{4} \left(\frac{\rho_M}{\rho_S} - 1\right) \left(\frac{Z}{R}\right)^3 - \frac{3}{4} \left(\frac{\rho_M}{\rho_S} - 1\right) \left(\frac{Z}{R}\right)^2 + \frac{\rho_M}{\rho_S} & 0 \leq Z \leq 2A \\ \frac{\rho_M}{\rho_S} & Z < 0 \end{cases} \quad [5]$$

A. Mechanical Model of an Inclusion Without Film Formation

If the Reynolds number is less than unity, no film will form because the speed of inclusions at the interface is low enough for there to be direct contact with the slag. The particle at the interface between steel and slag is acted upon by four forces: the buoyancy force, added-mass force, rebound force, and drag force.^[14,15] Figure 2 is a schematic of the situation. Re and the Stokes terminal velocity are defined as

$$Re = 2UA \frac{\rho_M}{\mu_M}, \quad [6]$$

$$U_{St} = \frac{2}{9} A^2 (\rho_M - \rho_I) \frac{g}{\mu_M}, \quad [7]$$

The buoyancy force involves a difference between relative densities, but must also account for the separate volumes of the inclusion that are within slag and the steel phase.

The buoyancy force is defined as

$$F_b = \frac{4}{3} \pi A^3 (\rho_S \tilde{\Delta}_b g - \rho_I g), \quad [8]$$

The value of $\tilde{\Delta}_b$ changed with the displacement of inclusion though Eq. [5].

The added-mass force is in the direction opposite to the acceleration and is given by

$$F_m = \frac{14}{23} \pi A^3 \rho_S \tilde{\Delta}_b \frac{d^2 z}{dt^2}, \quad [9]$$

The volume rate of the inclusion in metal and slag determines the magnitude and direction of the buoyancy force. If the density of the inclusion is lower than both that of the slag and that of the metal, the force is directed upward. If the inclusion is denser than the slag, the inclusion particle will stay at the bottom of the slag layer, such as in the case of a solid Al_2O_3 inclusion.

According to the assumption the Re number is less than unity when no film is around the inclusion. So the direction of drag force is opposite to the velocity which is defined as:

$$F_d = 6\pi A \mu_S \cdot \tilde{B} \cdot \frac{dZ}{dt}, \quad [10]$$

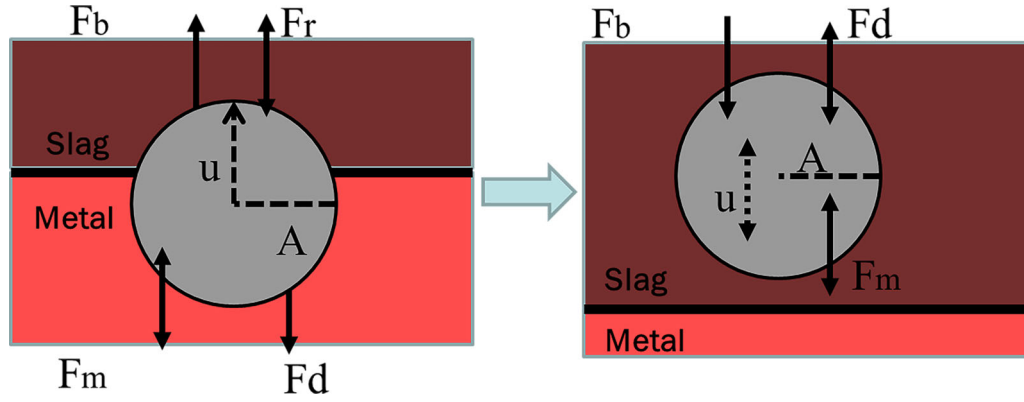


Fig. 2—Force analysis of an inclusion at the interface and in slag phase without film formation.

After the inclusion has transferred into the slag phase absolutely, the buoyancy force, drag force, and added-mass force will change as both $\tilde{\Delta}_b$ and \tilde{B} approach 1. So force analysis of the inclusion can be divided into two parts as following.

1. Force analysis of the inclusion at the interface

The rebound force is generated by the change in interfacial energy during the inclusion transfer across the interface. The interfacial energy is defined as

$$E_r = -\pi(2RZ - Z^2)\sigma_{MS} + 2\pi RZ\sigma_{SI} + 2\pi R(2R - Z)\sigma_{MI}, \quad [11]$$

The rebound force is thus

$$F_r = \frac{dE_r}{dZ} = (-2\pi A + 2\pi z)\sigma_{MS} + 2\pi A\sigma_{SI} - 2\pi A\sigma_{MI}, \quad [12]$$

2. Force analysis of the inclusion in slag

After the inclusion has transferred into the slag phase absolutely, the interfacial energy will be fixed, and the rebound force will thus be zero.

According to the model assumptions and Newton's second law, substituting Eqs. [8] through [10] and [12] into the Eq. [13].

$$F_b - F_d - F_r - F_m = \frac{4}{3}\pi A^3 \rho_1 \frac{d^2 Z}{dt^2}, \quad [13]$$

According to the above force analysis at the interface, when there is no formation of liquid film, the displacement of the inclusion before it transfers into the slag phase absolutely and after it transfers into the slag phase absolutely can be summarized as:

$$\frac{d^2 Z^*}{dt^{*2}} = \begin{cases} \frac{1}{(\rho_S \tilde{\Delta}_b + 2\rho_1)} \left[2(\rho_S \tilde{\Delta}_b - \rho_1) - \frac{3\sigma_{MS}}{A^2 g} (Z^* - 1 - \frac{\sigma_{MI} - \sigma_{SI}}{\sigma_{MS}}) - 6 \frac{\mu_S}{\sqrt{A^3 g}} \tilde{B} \frac{dZ^*}{dt^*} \right] & 0 < Z^* < 2 \\ \frac{2(\rho_S - \rho_1)}{\rho_S + 2\rho_1} - \frac{9\mu_S}{\sqrt{A^3 g} (\rho_S + 2\rho_1)} \frac{dZ^*}{dt^*} & Z^* \geq 2 \end{cases}, \quad [14]$$

B. Mechanical Model of the Inclusion with Film Formation

As mentioned earlier, a metal film will form between the inclusion particle and the interface if $Re \geq 1$. The particle is again acted upon by four forces: the buoyancy force, added-mass force, rebound force, and drag force.^[14,15]

When there is a metal film, the transfer of the inclusion can be divided into four parts: transference to the interface, separation into the slag phase or rebound back into the metal, re-entering of the interface, and separation into the slag phase or rest at the interface. Figure 3 is a schematic representation of the situation.

The model assumes that a metal film will form if the distance between the particle and interface, denoted as S_0 , is 0.002 A and that the film will rupture when the distance reduces to 0.001 A.

The buoyancy force in different distances is expressed as

$$F_b = \begin{cases} \frac{4}{3}\pi A^3 (\rho_M - \rho_1)g & Z < 2A \\ \frac{4}{3}\pi A^3 (\rho_S - \rho_1)g & Z \geq 2A \end{cases}, \quad [15]$$

The drag force is selected from Eq. [1] to Eq. [3] with the change of Re number. At the different distances, the force may also change with different value of $\tilde{\Delta}_b$ and \tilde{B} .

The added-mass force is expressed as

$$F_m = \begin{cases} \frac{2}{3}\pi A^3 \rho_M \frac{d^2 Z}{dt^2} & Z < 2A \\ \frac{4}{3}\pi A^3 \rho_S \frac{d^2 Z}{dt^2} & Z \geq 2A \end{cases}, \quad [16]$$

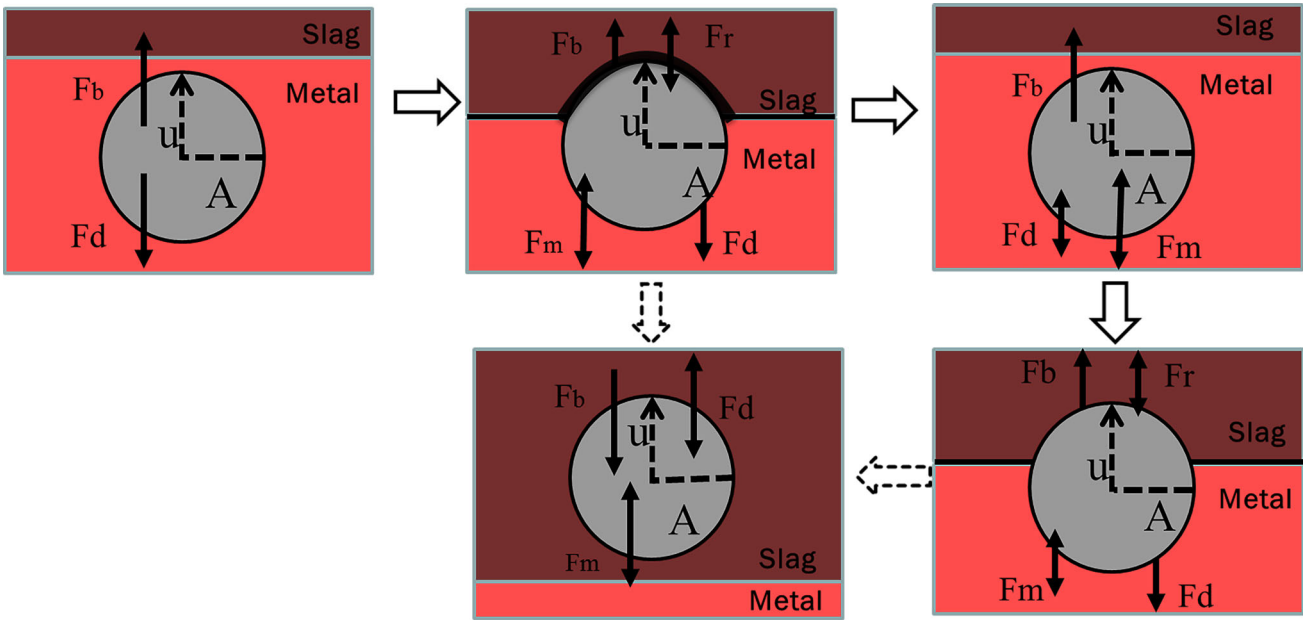


Fig. 3—Force analysis of an inclusion at the interface of metal phase and slag phase with film formation.

Force analysis of the inclusion can be divided into three parts as following during the motion process with a film formation.

1. Force analysis of the inclusion at the interface

The metal film thickness is S_0 at time t_0 . The rising distance of the inclusion, denoted as $Z(t)$, is a function of time t and the film thickness is denoted as $S(t)$, as shown in Figure 4. The angle θ_c in the figure ranges from 0 to π ; the inclusion is not in contact with the interface if the angle is zero and the inclusion separates absolutely into the slag if the angle is π .

μ_s is the slag viscosity, σ_{MS} is the interfacial tension between metal and slag, and S is the film thickness. The rebound force can be obtained by integrating Eq. [17]:

$$F_r = 4\pi A^2 \left[\frac{\sigma_{MS}}{2(A+S)} \sin^2 \theta_c + \frac{dZ}{dt} \frac{\mu_s}{3} \left(\frac{1}{A+2S} - \frac{1}{A+4S} \right) (1 - \cos^3 \theta_c) \right], \quad [18]$$

Substituting the expressions of the buoyancy force, added-mass force, and drag force into Newton's equation (Eq. [13]), the displacement of the inclusion before it transfers into the slag phase absolutely is expressed as:

$$\frac{d^2 Z^*}{dt^{*2}} = \begin{cases} \frac{1}{(\rho_M + 2\rho_I)} \left[f(S^*, Z^*) - h(S^*, A) \times \left[1 - \left(\frac{1-Z^*}{1+S^*} \right)^3 - \frac{9\mu_M}{\sqrt{A^3 g}} \frac{dZ^*}{dt^*} \right] \right] & 1 < Re \leq 8 \\ \frac{1}{(\rho_M + 2\rho_I)} \left[f(S^*, Z^*) - h(S^*, A) \times \left[1 - \left(\frac{1-Z^*}{1+S^*} \right)^3 - \frac{9\mu_M(1+0.15Re^{0.687})}{\sqrt{A^3 g}} \frac{dZ^*}{dt^*} \right] \right] & 8 < Re \leq 5, \\ \frac{1}{(\rho_M + 2\rho_I)} \left[f(S^*, Z^*) - h(S^*, A) \times \left[\left[1 - \left(\frac{1-Z^*}{1+S^*} \right)^3 \right] \frac{dZ^*}{dt^*} - 0.33\rho_M \left(\frac{dZ^*}{dt^*} \right)^2 \right] \right] & Re > 500 \end{cases} \quad [19]$$

According to the Nakajima's model, when the interface is deformed, the continuity of normal stress across the film interface is given by

$$\begin{aligned} P_{\text{Film}} - P_{\text{Slag}} &\cong P_{\text{Film}} - P_{\text{Metal}} = \frac{2\sigma_{MS}}{A+S} - 2\mu_s \frac{\partial v_r}{\partial r} \Big|_{r=A+S} \\ &= \frac{2\sigma_{MS}}{A+S} + \frac{dZ}{dt} 2\mu_s \left[\frac{1}{A+S} - \frac{3}{A+4S} \right] \cos \theta \end{aligned} \quad [17]$$

where P_{Film} is the pressure of the metal film, P_{Slag} is the pressure of the slag, P_{Metal} is the pressure of the metal,

$$\begin{aligned} \text{where } f(S^*, Z^*) &= 2(\rho_M - \rho_I) - \frac{3\sigma_{MS}(2+S^*-Z^*)(S^*+Z^*)}{A^2 g (1+S^*)^3}, \\ h(S^*, A) &= \frac{3\mu_s}{\sqrt{A^3 g}} \left(\frac{1}{1+2S^*} - \frac{1}{1+4S^*} \right). \end{aligned}$$

2. Force analysis of an inclusion in metal

The inclusion may rebound back into the metal phase. The interfacial energy is fixed when the inclusion is in the slag phase absolutely, and the rebound force will thus be zero.

The displacement of the inclusion that rebounds into the metal phase will be

$$\frac{d^2 Z^*}{dt^{*2}} = \begin{cases} \frac{2(\rho_M - \rho_I)}{\rho_M + 2\rho_I} - \frac{9\mu_M}{\sqrt{A^3 g} (\rho_M + 2\rho_I)} \frac{dZ^*}{dt^*} & 1 < \text{Re} \leq 8 \\ \frac{2(\rho_M - \rho_I)}{\rho_M + 2\rho_I} - \frac{9(1+0.15\text{Re}^{0.687})\mu_M}{\sqrt{A^3 g} (\rho_M + 2\rho_I)} \frac{dZ^*}{dt^*} & 8 < \text{Re} \leq 500, \\ \frac{2(\rho_M - \rho_I)}{\rho_M + 2\rho_I} - \frac{0.33\rho_M}{(\rho_M + 2\rho_I)} \left(\frac{dZ^*}{dt^*}\right)^2 & \text{Re} > 500 \end{cases} \quad [20]$$

The inclusion will re-enter the interface owing to its density being lower than that of the metal phase. If the velocity is low enough that $\text{Re} < 1$, the inclusion will transfer through the interface as no film forms, or there will be a film forming.

3. Force analysis of an inclusion in slag

Due to the different values of Re , the displacement of the inclusion in the slag phase will be

$$\frac{d^2 Z^*}{dt^{*2}} = \begin{cases} \frac{2(\rho_M - \rho_I)}{\rho_M + 2\rho_I} - \frac{9\mu_S}{\sqrt{A^3 g} (\rho_M + 2\rho_I)} \frac{dZ^*}{dt^*} & 1 < \text{Re} \leq 8 \\ \frac{2(\rho_M - \rho_I)}{\rho_M + 2\rho_I} - \frac{9(1+0.15\text{Re}^{0.687})\mu_S}{\sqrt{A^3 g} (\rho_M + 2\rho_I)} \frac{dZ^*}{dt^*} & 8 < \text{Re} \leq 500, \\ \frac{2(\rho_M - \rho_I)}{\rho_M + 2\rho_I} - \frac{0.33\rho_M}{(\rho_M + 2\rho_I)} \left(\frac{dZ^*}{dt^*}\right)^2 & \text{Re} > 500 \end{cases} \quad [21]$$

The equation for the drainage of the metal film δ is obtained from the expression for the film surface:

$$\delta = \int_0^{\theta_c} (2\pi A \sin \theta) A d\theta = -2\pi A^2 (\cos \theta - 1) = 2\pi A^2 \frac{S + Z}{A + S}, \quad [22]$$

The continuity of the film flow is expressed as

$$\delta \sigma - U(2\pi A \sin \theta_C) S dt = (S + dS)(\delta + d\delta), \quad [23]$$

The film flow-out velocity is

$$U = -\frac{1}{r \sin \theta} \frac{d\psi}{dr} = -\frac{dZ}{dt} \sin \theta_C, \quad [24]$$

The drainage of the steel film per unit time in dimensionless variables is

$$\frac{dS^*}{dt^*} = \frac{1}{2S^* + Z^*} \left[-\frac{dZ^*}{dt^*} (2 - Z^*) (S^* + Z^*) S^* - S^* \frac{dZ^*}{dt^*} \right], \quad [25]$$

The dimensionless displacement, steel film thickness, time, velocity, and acceleration in the above equation are expressed as

$$Z^* = \frac{Z}{A}, \quad [26]$$

$$S^* = \frac{S}{A}, \quad [27]$$

$$t^* = t \sqrt{\frac{g}{A}}, \quad [28]$$

$$\frac{dZ^*}{dt^*} = \sqrt{\frac{1}{Ag}} \frac{dZ}{dt}, \quad [29]$$

$$\frac{d^2 Z^*}{dt^{*2}} = \frac{1}{g} \frac{d^2 Z}{dt^2}, \quad [30]$$

III. MODEL VALIDATION

This investigation validated the numerical model using a water model. The system of inclusion movement at the interface between slag and metal was represented by the wetting interaction of the inclusion, metal, and slag. The capillary length in the simulation system must therefore be similar to those of the numerical system.

A. Similarity of the Capillary Length

The capillary length is a characteristic length of the interface between two fluids, and is determined by the acceleration due to gravity and interfacial tension in hydromechanics:

$$\lambda = \sqrt{\frac{\sigma}{\rho g}}, \quad [31]$$

where σ is the interfacial tension between liquids, ρ is the density of fluid, and g is acceleration due to gravity.

The capillary lengths of the interface between slag and metal and the interface between oil and water in the water model are defined as

$$\lambda_{\text{metal-slag}} = \sqrt{\frac{\sigma_{\text{ms}}}{\Delta \rho_{\text{ms}} g}}, \quad [32]$$

$$\lambda_{\text{water-oil}} = \sqrt{\frac{\sigma_{\text{wo}}}{\Delta \rho_{\text{wo}} g}}, \quad [33]$$

In this investigation, the capillary length of the interface between slag and metal ($\lambda_{\text{metal-slag}}$) was 0.58 m, and that of the interface between water and oil ($\lambda_{\text{water-oil}}$) was 0.6 m. These two capillary lengths are similar and it is thus reasonable to use the interface between water and oil in simulating the interface between metal and slag.

B. Experimental Design

The materials used in the experiment were silicon oil AK 50, silicon oil AK 75, and hollow aluminum beads with diameters of 4 mm. The physical properties of the materials are listed in Table I.

The main pieces of equipment used in the experiment were a Fastec Hispec 5 high-speed camera, Xcitex ProAnalyst Professional Ultra Bundle Motion Analysis Software, and a tank constructed of half-inch-thick clear polycarbonate. In the experiment, opening the switch at the bottom of containers and rotating the net baffle allowed the hollow aluminum beads to float upward from the bottom of the tank. The high-speed camera was used to record the movement of the particles at the interface between oil and water. Figure 5 is a schematic of the experiment. The velocity of the particle at the interface could be analyzed with the Xcitex ProAnalyst software.

1. Numerical solution

The expressions depicting the inclusion movement in model are all second-order differential equations. Solve these motion equations with C programming language, the R-K solution with fourth-level and fourth-order is used to obtain the numerical solutions.

$$\begin{cases} y_{i,n+1} = y_{i,n} + \frac{h}{6}(k_{1,i} + 2k_{2,i} + 2k_{3,i} + k_{4,i}) \\ k_{1,i} = f_i(x_n, y_{1,n}, \dots, y_{m,n}) \\ k_{2,i} = f\left(x_n + \frac{h}{2}, y_{1,n} + \frac{h}{2}k_{1,1}, \dots, y_{m,n} + \frac{h}{2}k_{1,m}\right) \\ k_{3,i} = f\left(x_n + \frac{h}{2}, y_{1,n} + \frac{h}{2}k_{2,1}, \dots, y_{m,n} + \frac{h}{2}k_{2,m}\right) \\ k_{4,i} = f\left(x_n + \frac{h}{2}, y_{1,n} + \frac{h}{2}k_{3,1}, \dots, y_{m,n} + \frac{h}{2}k_{3,m}\right) \end{cases} \quad [34]$$

The velocity of the particle could be calculated by the software, and speed curves of the particles at the interface between water and oil thus drawn. At the same time, the theoretical speed curves could be determined by substituting the parameters of the water model into the theoretical model. The speed curves of the particles at the interface between water and oil and the theoretical speed curves could thus be compared.

According to the model, the Re number of the hollow aluminum beads is larger than 500, and there will be a film formation between the inclusion particle and the interface. So the displacement of the inclusion at the interface and after it transfers into the slag phase absolutely can be calculated respectively by Eq. (35).

$$\frac{d^2 Z^*}{dt^{*2}} = \begin{cases} \frac{1}{(\rho_M + 2\rho_I)} \left[f(S^*, Z^*) - h(S^*, A) \times \left[\left[1 - \left(\frac{1 - Z^*}{1 + S^*} \right)^3 \right] \frac{dZ^*}{dt^*} - 0.33\rho_M \left(\frac{dZ^*}{dt^*} \right)^2 \right] \right] & Z < 2A \\ \frac{2(\rho_M - \rho_I)}{\rho_M + 2\rho_I} - \frac{0.33\rho_M}{(\rho_M + 2\rho_I)} \left(\frac{dZ^*}{dt^*} \right)^2 & Z \geq 2A \end{cases} \quad [35]$$

The speed curves of the particles at the interface between water and two kinds of oils in the water model experiment are shown in the Figures 6 and 8. Figures 7 and 9 compare the experimental curves and theoretical calculation curves. Both results agree consistently by comparison. However, there are fluctuations in the experimental curves, possibly due to the rough surface of aluminum bead. Due to the rough surface, the draining of water film from the particle surface is too slow to make the assumption that the deformed interface instantaneously reforms itself to a flat interface after film rupture, though the velocity may go negative, the inclusion still is on the interface and the inclusion finally stay on the interface stably. Moreover, the final speed is slightly oscillating and near 0 in the experimental curves, this may be due to the fluctuation of the liquid interface during the experiment.

IV. ANALYSIS OF PRELIMINARY RESULTS

Depending on whether Re is above or below unity, inclusions move at the steel–slag interface with or without the formation of a film; a film forms between the inclusion and interface when $Re > 1$.

When the Stokes terminal velocity is selected as the terminal velocity of the inclusion, the viscosity of the slag is 0.08 Pa·s, the interfacial tension between the slag and inclusion is 0.24 N/m, the viscosity of the metal is 0.006 Pa·s, the density of the metal is 7000 kg/m³, and the density of an Al₂O₃ inclusion is 3990 kg/m³; it is calculated that no film forms when the inclusion size is less than 150 μm but that a film does form between the inclusion and interface otherwise. And the thermodynamic property parameters of the material are listed in the Table II.

Through the model calculation, we obtain the relationship between displacement and time as shown in Figure 10. Figures 10(b) and (d) show that, if the size of the inclusion ranges from 150 to 190 μm, the inclusion rebounds to the metal under the effect of the film, and the separation time is significantly longer. When the inclusion size is greater than 190 μm (Figure 10(e)), the inclusion crosses the interface directly without rebounding, which decreases the separation time obviously.

In the model, the size of inclusions at slag–metal interface is assumed as the constant. The effect of dissolution on the size of inclusions at slag–metal interface is discussed firstly to check the validity of assumption in the model. Based on the fact that the separation process of inclusions could not be observed

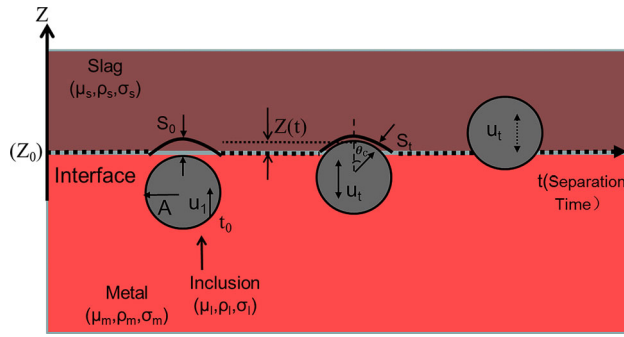


Fig. 4—Motion of an inclusion with formation of a metal film.

Table I. Physical Properties of Materials

	Density (kg/m ³)	Viscosity (Pa·s)	Interfacial Tension Against H ₂ O (N/m)	Interfacial Tension Against Oil (N/m)
Silicon oil AK 50	960	0.023	0.041	—
Silicon oil AK 75	962	0.072	0.049	—
Water	1000	0.00089	—	—
Hollow aluminum	670	—	0.614	AK 50 0.629 AK 75 0.631

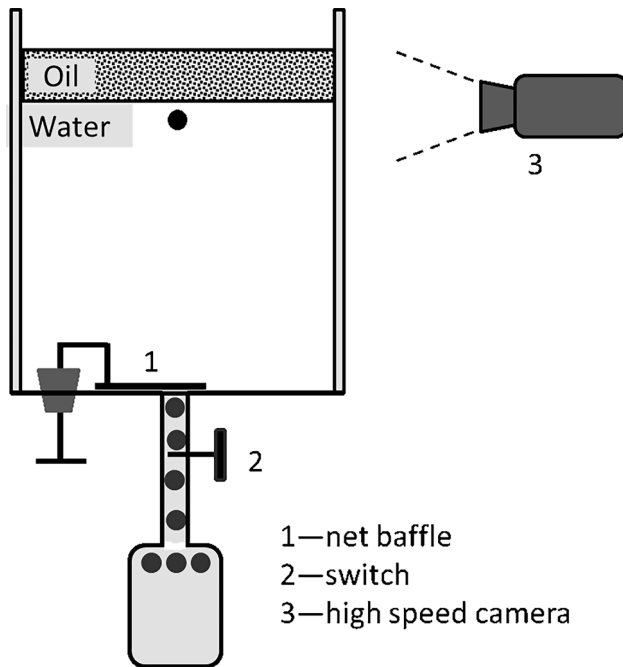


Fig. 5—Schematic of the experimental equipment.

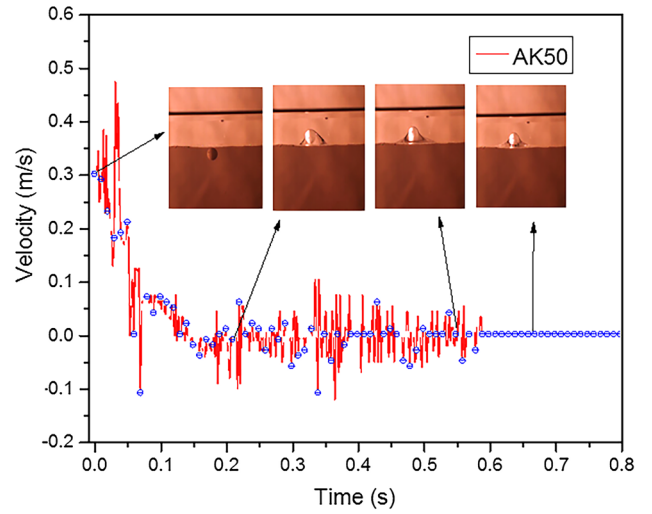


Fig. 6—Experimental speed curve of the hollow aluminum bead at the interface between water and oil.

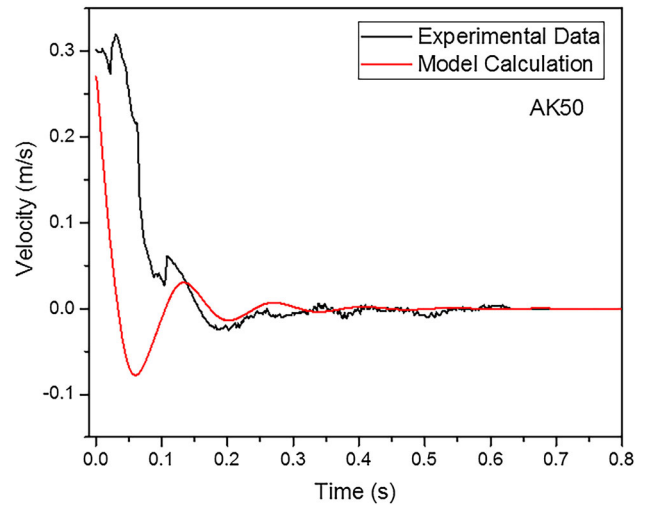


Fig. 7—Theoretical speed curve.

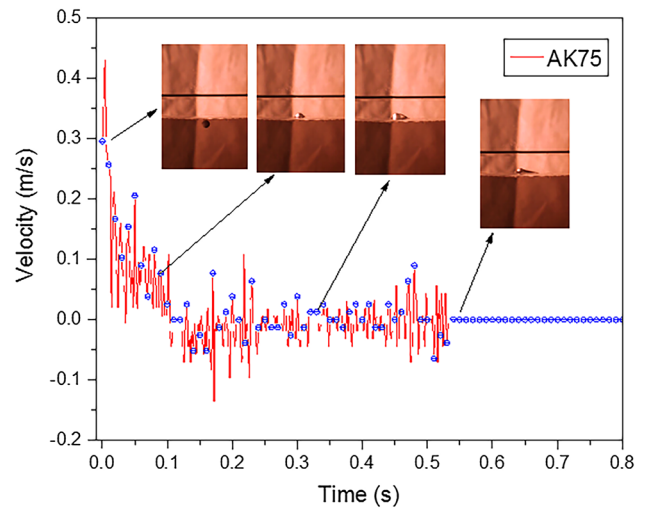


Fig. 8—Experimental speed curve of the hollow aluminum bead at the interface between water and oil.

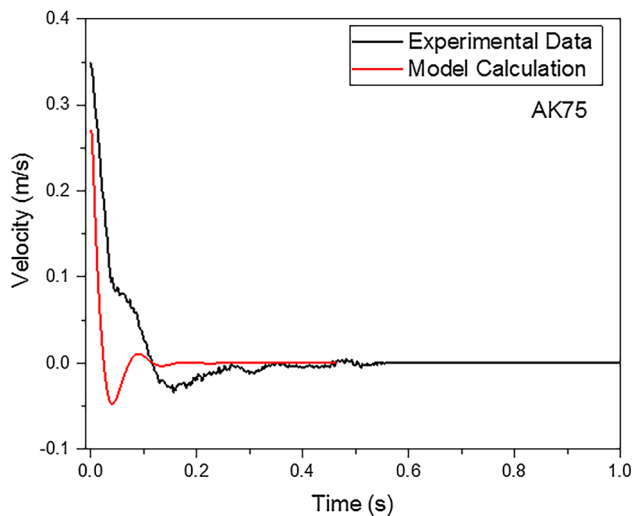


Fig. 9—Theoretical speed curve.

with confocal scanning laser microscopy, Sridhar^[3,27–31] claimed that the separation rate was not observable. However, the dissolution process of solid inclusions could be observed in the experiment, the dissolution time of a 100 μm Al_2O_3 inclusion in slag (46.6 wt pct Al_2O_3 , 51.5 wt pct CaO, 0.50 wt pct MgO, and 1.3 wt pct SiO_2) is about 75 seconds. The diffusion time τ can be calculated by S. Sridhar's model:^[17]

$$\tau = \frac{\rho \cdot R_0^2 \cdot 3\pi a \eta}{2kT\Delta C}, \quad [36]$$

where ρ —the particle density; ΔC —the driving force of the dissolution; k —the Boltzmann constant; T —the temperature; a —the ionic diameter; η —the viscosity of the slag. The separation time of a 150 μm inclusion is about 2.6 ms (in Figure 10) which is far shorter than the dissolution time. Thus the assumption which regards the inclusion size at the separation process as

a constant is reasonable. However, the dissolved dynamics of inclusions at steel–slag interface needs further study.

V. SUMMARY AND CONCLUSION

A mathematical model predicting the motion behavior of nonmetallic inclusions at the interface of molten steel and slag was established. The model considers all factors affecting the motion of inclusions at the interface and in areas nearby and the effect of fluid flow containing inclusions with the drag force of different Re numbers, overcoming the limitation of previous models that only consider the forces acting on nonmetal inclusions at the interface, and assume that the fluid flow containing inclusions is Stokes flow regardless of the value of Re. The model established here also considers cases in which the inclusions enter the slag interior and are rebounded into the molten steel again. The displacement–time curve obtained from the mathematical model to describe the motion behavior of inclusions at the interface and in nearby areas was verified with a physical water model, with the results showing good agreement.

The preliminary calculation results show that a liquid film forms at the inclusion surface only when the inclusion is large enough. For Al_2O_3 inclusions floating upward to the steel–slag interface at Stokes terminal velocity, the critical size for the generation of liquid film is 150 μm . Inclusions with liquid film at their surfaces are rebounded into the steel when their size is within a certain range, and beyond the size range, the inclusions can enter the slag phase directly. In the case of the Al_2O_3 inclusion, when adopting the Stokes floatation velocity as the terminal velocity, the viscosity of slag as 0.08 Pa·s and the interfacial tension between inclusions and slag as 0.24 N/m, the inclusion will be rebounded at the interface under the effect of liquid film if the diameter lies in the range of 150–190 μm . However, an Al_2O_3 inclusion larger than 190 μm can pass through the steel–slag interface and enter the slag phase.

Table II. Thermodynamic Property Parameters of the Material

	Density (kg/m^3)	Viscosity (Pa·s)	Interfacial Tension (N/m)	Interfacial Tension (N/m)	Composition			
Metal	7000 ^[14]	0.006 ^[14]	σ_{IS} 0.01–0.6 ^[25]	σ_{M} 1.606 ^[26]	Fe:100 pct			
Inclusion	3990 ^[14]	–	σ_{IM} 1.504 ^[14]	σ_{I} 0.650 ^[24]	Al_2O_3 :100 pct			
Slag	2720 ^[24]	0.08 ^[23]	σ_{MS} 1.43 ^[24]	σ_{S} 0.415 ^[24]	SiO_2	CaO	Al_2O_3	MgO
					25	55	10	2

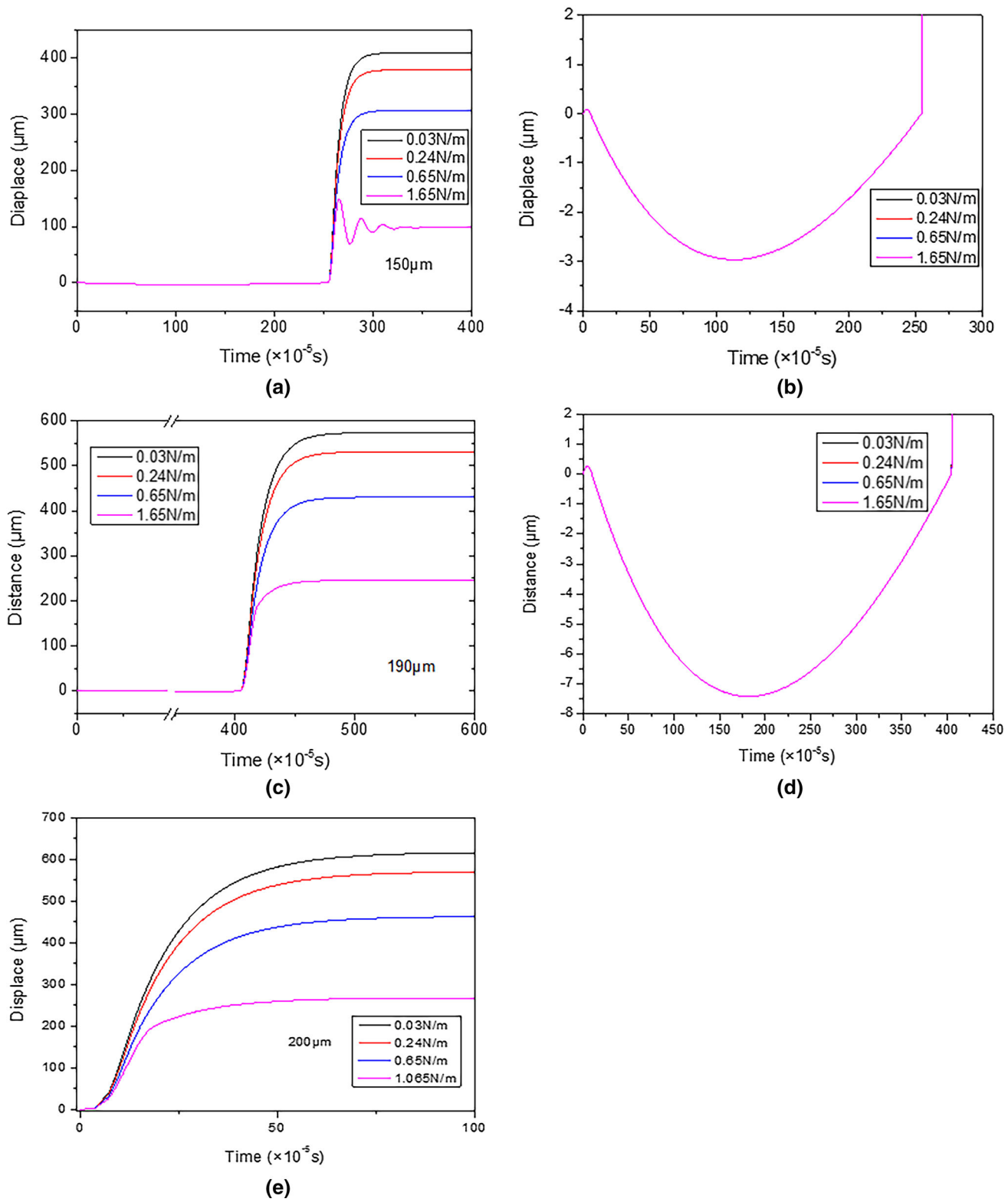


Fig. 10—Displacement curves of hollow aluminum beads.

ACKNOWLEDGMENTS

The authors gratefully acknowledge financial support from National Science Foundation of China (Nos. 51474076 and 51304016) and National Basic Research Program of China (973 Program) (No. 2014CB643300).

OPEN ACCESS

This article is distributed under the terms of the Creative Commons Attribution 4.0 International License (<http://creativecommons.org/licenses/by/4.0/>), which permits unrestricted use, distribution, and reproduction in any medium, provided you give appropriate credit to the original author(s) and the source, provide a link to the Creative Commons license, and indicate if changes were made.

NOMENCLATURE

Z	Displacement of the inclusion particle, m
$Z(0)$	Initial position of the inclusion, m
S	Metal film thickness, m
$S(0)$	Initial thickness of the metal film, m
t	Time s
Re	Reynolds number
U	Terminal velocity of the inclusion particle, m/s
U_{St}	Stokes terminal velocity, m/s
A	Radius of the particle, m
ρ_x	Density, kg/m ³
μ_x	Viscosity, Pa·s
g	Gravitational acceleration, m/s ²
E_r	Interfacial energy, J
σ_{xy}	Interfacial tension, N/m
P_x	Pressure, Pa

SUBSCRIPTS

M	Metal
S	Slag
I	Inclusion

SUPERSCRIPT

* Dimensionless

REFERENCES

1. W.C. Leslie: *ISS Trans.*, 1983, vol. 2, pp. 1–24.
2. A.W. Cramb: in *Impurities in Engineering Materials*, C.L. Briant, ed., Marcel Dekker, New York, 1999, pp. 49–89.
3. S.H. Lee, C. Tse, K.W. Yi, P. Misra, V. Chevrier, C. Orrling, S. Sridhar, and A.W. Cramb: *J. Non-Cryst. Solids*, 2001, vol. 282, pp. 41–48.
4. J. Wikström, K. Nakajima, L. Jonsson, and P. Jönsson: *Steel Res. Int.*, 2008, vol. 79, pp. 826–34.
5. A. Ramos-Banderas, R.D. Orales, L. García-Demedices, and M. Díaz-Cruz: *Iron Steel Inst. Jpn. Int.*, 2003, vol. 45, pp. 653–62.
6. W. Li-Tao and X.U.E. Zheng-liang: *J. Iron Steel Res. Int.*, 2005, vol. 17, p. 36.
7. M. Hallberg, P.G.M. Hallberg, P.G. Jönsson, T.L.I. Jonsson, and R. Eriksson: *Scand. J. Metall.*, 2005, vol. 34, p. 41.
8. Y. Miki and B.G. Thomas: *Metal. Mater. Trans. B*, 1999, vol. 30B, p. 639.
9. P. Kozakevitch and M. Olette: *Rev. Met. Paris*, 1971, vol. 68, p. 636.
10. P. Kozakevitch and M. Olette: *The Iron and Steel Institute*, London, 1970, pp. 42.
11. P.V. Riboud and M. Olette: in *Proc. 7th In. Conference on Vacuum Metallurgy*, Tokyo, 1982, pp. 879.
12. A.W. Cramb and J. Jimbo: in *W. O. Philbrook Memorial Symp. METEC Congr. ISS, Warrendale, PA*, 1988 pp. 259.
13. K. Nakajima and K. Okamura: in *4th Int. Conf. on Molten Slags and Fluxes, ISIJ*, Sendai, 1992, pp. 505.
14. J. Strandh, K. Nakajima, R. Eriksson, and P. Jönsson: *Iron Steel Inst. Jpn. Int.*, 2005, vol. 45, pp. 1838–39.
15. J. Strandh, K. Nakajima, R. Eriksson, and P. Jönsson: *Iron Steel Inst. Jpn. Int.*, 2005, vol. 45, pp. 1597–98.
16. J.W. Cleaver and B. Yates: *J. Coll. Interface Sci.*, 1973, vol. 44, pp. 464–474.
17. Martin. Valdez, George.S. Shannon, and Seetharaman. Sridhar: *Iron Steel Inst. Jpn. Int.*, 2006, vol. 46, pp. 450–57.
18. D. Bouris and G. Bergeles: *Metal. Mater. Trans. B*, 1988, vol. 29B, pp. 641–49.
19. R.D. Morales, S. Lopez-Ramirez, Palafox-Ramos *et al.*: *Iron Steel Inst. Jpn. Int.*, 1999, vol. 39 (5), p. 455.
20. K. Cukierski and B.G. Thomas: *Metal. Mater. Trans. B*, 2008, vol. 39B, p. 94.
21. Z. Yan: *Theory of low Reynolds-number flows*, Peking University Press, Beijing, 2002.
22. R. Clift, J.R. Grace, and M.E. Weber: *Bubbles, Drops, and Particles*, Academic Press Inc, New York, NY, 2005, p. 111.
23. M.-Y. Zhu, I. Sawada, and N. Yamasaki: *Iron Steel Inst. Jpn. Int.*, 1996, vol. 36, p. 506.
24. Verein Deutscher Eisenhüttenleute, *Slag Atlas 2nd Edition*, Verlag Stahleisen GmbH, 1995.
25. George Newlin Shannon: D.D. Thesis, Department of Materials Science and Engineering Carnegie Mellon University, Pittsburgh, 2007.
26. Sami Jani: M.D. Thesis, Stockholm University. Sweden, 2007.
27. M. Valdez, K. Prapakorn, A.W. Cramb, and S. Sridhar: *Steel Res.*, 2001, vol. 72, pp. 291–97.
28. M. Valdez, K. Prapakorn, A.W. Cramb, and S. Sridhar: *Iron-making Seelmaking*, 2002, vol. 29 (1), pp. 47–52.
29. S. Sridhar and A.W. Cramb: *Metall. Mater. Trans. B*, 2000, vol. 31B, pp. 406–10.
30. A.B. Fox, M.E. Valdez, J. Gisby, R.C. Atwood, P.D. Lee, and S. Sridhar: *ISIJ Int.*, 2004, vol. 44 (5), pp. 836–45.
31. P. Misra, V. Chevrier, S. Sridhar, and A.W. Cramb: *Metall. Mater. Trans. B*, 2000, vol. 31B, pp. 1135–39.